

Spatial topological insulator

Qinghua He¹, Wenlong Gao², and Feng Liu^{3,4*}

¹*Institute of High Pressure Physics, School of Physical Science and Technology, Ningbo University, Ningbo 315-211, China*

²*Eastern Institute of Technology, Ningbo, China*

³*Department of Nanotechnology for Sustainable Energy, School of Science and Technology, Kwansai Gakuin University, Gakuen 2-1, Sanda 669-1337, Japan and*

⁴*Department of Physics, Shaoxing University, Shaoxin 312-000, China*

Traditional topological insulators often rely on band inversions driven by nonuniform hopping textures and spin-orbit coupling, as exemplified in the Su-Schrieffer-Heeger and Kane-Mele models. We present a novel approach utilizing the spatial nature of sublattice symmetry to induce nontrivial topological insulating properties characterized by second-order corner states without band inversion. To substantiate our proposal, we design a photonic crystal with non primitive translational symmetry, demonstrating unique directional waveguide edge modes and localized corner modes.

Topology plays a pivotal role in condensed matter physics, distinguishing materials that, despite similar energy band structures, exhibit fundamentally different properties [1–3]. In particular, robust edge states [4–8] and corner states [9–13] emerge at the interfaces of topologically distinct finite samples, protected by nontrivial topological invariants. These invariants are typically associated with band inversions [14], which can be delineated through the decomposition of elementary band representations [15, 16]. In strong topological insulators, the band structures defy an elementary band representation, thereby impeding the construction of Wannier functions [17]. In contrast, weak topological insulators feature well-defined Wannier functions with centers that do not align with atomic sites [18, 19]. Under the constraint of time-reversal symmetry, band inversions are achievable by either adjusting hopping amplitudes among atomic sites, as in the Su-Schrieffer-Heeger model [20, 21], or by introducing spin-orbit coupling, exemplified by the Kane-Mele model [22, 23].

In addition to the well-known band inversion scenario, the crucial role of the spatial nature of sublattice symmetry in topological insulators has been largely overlooked [24, 25]. The spatial nature of sublattice reveals when there exists a non primitive translational symmetry that alternates sublattice labels, leading to a doubling of bands that may exhibit nontrivial topological properties.

In this Letter, we demonstrate that enforcing non primitive translational symmetry along the diagonal and off-diagonal directions of the unit cell enables a strong topological insulator characterized by both topological edge and corner states. This approach diverges from conventional methods that require fine-tuning of the hopping amplitude ratio or the introduction of spin-orbit coupling. Instead, the non primitive translational symmetry naturally produces a coexistence of trivial and nontrivial bands with nonequivalent Wannier centers below a band gap.

The schematic representation of the tight-binding model we propose is illustrated in Fig. 1. Panels (a), (b) show the doubled unit cell and the primitive unit cell, respectively. For simplicity, we set the lattice constant of the doubled unit cell to 1, and the one of the primitive cell to $1/\sqrt{2}$. In the doubled unit cell, there are unique translational sym-

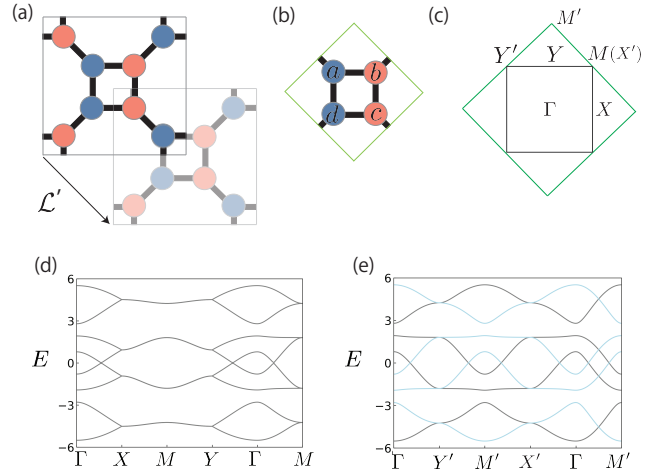


FIG. 1. (a) Schematic of the doubled unit cell. \mathcal{L} indicates a half translation along the diagonal direction. (b) Primitive unit cell of (a) due the L symmetry. (c) First Brillouin zone for the unit cells of (a) and (b). (d) Energy spectrum of the doubled unit. (e) Energy spectrum of the primitive unit cell, where the lighter lines is $E(k_x + 2\pi, k_y)$.

metries such that $\mathcal{L}' : (x, y) \rightarrow (x + 1/2, y - 1/2)$ and $\mathcal{L} : (x, y) \rightarrow (x + 1/2, y + 1/2)$. These symmetries swap the labels of the sublattices along the diagonal and off-diagonal directions, keeping the periodic structure unchanged as depicted in Fig. 1(a). Consequently, this arrangement results in a primitive cell with a reduced area, as shown in Fig. 1(b).

The Hamiltonian of the primitive cell in the momentum space can be written as

$$\hat{\mathcal{H}} = \begin{pmatrix} \mu & t & t'e^{-i\frac{k_x - k_y}{2}} & t \\ t & -\mu & t & t'e^{i\frac{k_x + k_y}{2}} \\ t'e^{i\frac{k_x - k_y}{2}} & t & -\mu & t \\ t & t'e^{-i\frac{k_x + k_y}{2}} & t & \mu \end{pmatrix}, \quad (1)$$

where t, t' are the intracell and intercell hopping amplitudes, respectively, $\pm\mu$ are the onsite potentials of the sublattices,

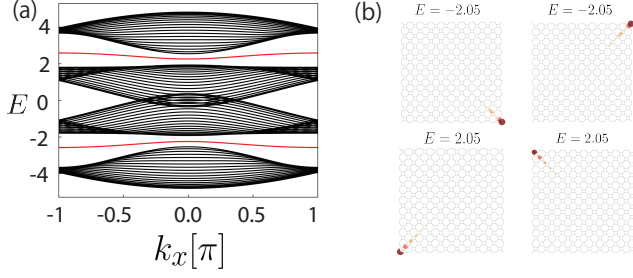


FIG. 2. (a) Ribbon spectrum of the doubled unit cell. (d) Four corner states of a finite sample of the doubled unit cell.

and the bases are four atomic sites as a, b, c, d denoted in Fig. 1(b). In momentum space, sublattice symmetry \mathcal{C} imposes a glide symmetry on the energy band structure, that is, $E(\mathbf{k}) \rightarrow -E(\mathbf{k} + 2\pi)$ with 2π acting in the k_x or k_y direction. In the following discussion, we take the k_x direction as an example. It is noted that, acting on momentum space, \mathcal{C} changes k_x by 2π [25].

Figure 1(c) illustrates the first Brillouin zones (BZs) for the primitive and doubled unit cells. The larger BZ associated with the primitive cell can be folded back to the doubled unit cell by shifting $\pm 2\pi$ along the k_x or k_y direction. The energy spectra along the high-symmetric lines in the first BZs of the two types of unit cells are displayed in Figs. 1(d) and (e). In Fig. 1(d), it is noted that at the fold-invariant k points, the energy bands are doubly degenerate in the doubled unit cell. In Fig. 1(e), both the $E(\mathbf{k})$ and $E(\mathbf{k} + 2\pi)$ branches are plotted to demonstrate the glide symmetry.

Because of the band doubling in the doubled unit cell, we can define a spatial-reversal pair as:

$$\begin{aligned} \mathcal{S}|u^I(k_x, k_y)\rangle &= R(-k_x, -k_y)|u^{II}(-k_x, -k_y)\rangle \\ \mathcal{S}|u^{II}(-k_x, -k_y)\rangle &= e^{i(k_x + k_y)} R^\dagger(k_x, k_y)|u^I(k_x, k_y)\rangle, \end{aligned} \quad (2)$$

where $\mathcal{S} = \mathcal{L}K$ with K the complex conjugation, and R is a unitary operator. At the fold-invariant k points we have $\mathcal{S}^2 = -1$, similarly to the time-reversal pair.

Here we argue that \mathcal{S} symmetry could yield a nontrivial topology. Assuming that the Wannier center of $|u^I\rangle$ is $\mathbf{P}^I = (W_x, W_y)$, then the Wannier center of $|u^{II}\rangle$ must be $\mathbf{P}^{II} = ((W_x - 1/2) \bmod 1, (W_y - 1/2) \bmod 1)$, as they actually originate from the same primitive cell. Then one sees that the spatial-reversal polarization is given as [5]

$$\mathbf{P}^\theta = \mathbf{P}^I - \mathbf{P}^{II} = \left(\frac{1}{2}, \frac{1}{2}\right). \quad (3)$$

It is noted that, unlike the time-reversal polarization, the finite \mathbf{P}^θ cannot be gauged out due to its spatial nature. The edge states emerge if $\mathbf{P}^I + \mathbf{P}^{II}$ is finite such that $W_x \neq \pm 1/4$ and $W_y \neq \pm 1/4$. Also, we have that $P_x^\theta + P_y^\theta = 1$. This suggests that \mathbf{P}^θ crosses $1/2$ when its direction changes from x to y , implying the existence of corner states. Different from the

conventional band inversion scenario, the topological classification here is largely determined by \mathcal{L} rather than the parameters such as hopping amplitudes and onsite energies.

In addition to \mathbf{P}^θ , the topology of the proposed model can be seen more transparently if the system possesses extra symmetry such as C_2 point group symmetry. In this case, there are $\{\mathcal{L}K, C_2\} = 0$ at the X and Y points, and $[\mathcal{L}K, C_2] = 0$ at the Γ and M points. The anticommutative and commutative relations of $\mathcal{L}K$ and C_2 guarantee that the doubling bands have opposite parities at the points X and Y while the same parity at the points Γ and M . Thus, in terms of the filling anomaly, we have $\chi^{(2)} = (1, 1, 0)$, which indicates the existence of corner modes [26].

Figure 2(a) presents the ribbon energy spectrum of the doubled unit cell configuration, where the ribbon is periodic along the x -direction and open along the y -direction. The red line indicates the edge states. Note that the edge states are not gapless because the open boundary adopted here breaks \mathcal{L} along the edge, similar to the time-reversal breaking case of quantum spin Hall effect (the connection between the valence and conduction bands is restored in the latter discussion for the proposed photonic crystal structure).

Figure 2(b) displays the corner state in a finite sample consisting of doubled unit cells, where the labels indicate their eigenenergies. It is noted that, as long as the \mathcal{S} symmetry is present, the corner state always exists regardless of the parameters. Here we set $\mu = 1.0$, $t = -1.4$ and $t' = -1.8$.

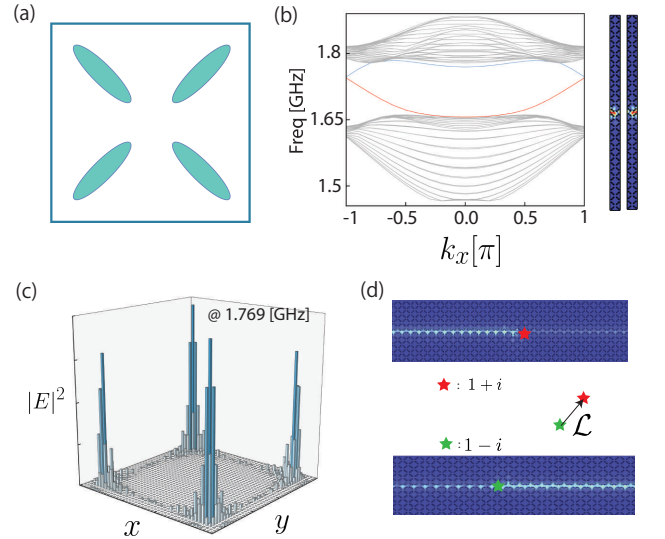


FIG. 3. (a) Unit cell of the photonic crystal with \mathcal{L} symmetry. (b) Ribbon spectrum of the photonic crystal. The topological interface is built between the unit cell of (a) and a half period shift of the unit cell in (a). Inset are the degenerate topological interfacial states for $k_x = \pi$. (c) Field distribution of the corner state at eigenfrequency 1.769[GHz]. (d) Selective excitation of edge states with opposite propagation directions. The sources for different propagation directions are separated by \mathcal{L} with opposite phases, i.e., $1 + i$ and $1 - i$.

For the experimental realization of our proposed model, one can search for materials within nonsymmorphic groups or compose an artificial crystalline structure such as a dielectric photonic crystal possessing \mathcal{L} . Figure 3(a) shows a possible design of the photonic crystal, where the colorful ellipses have a dielectric constant of 11. Figure 3(b) is the ribbon spectrum of the designated photonic crystal. Unlike the tight-binding case, the topological interface is built between two types of ribbons with the unit cell in (a) and the unit cell by a half-period shift of the unit cell in (a). In this way, two topological edge states emerge in a pair and are degenerate at fold-invariant k points, as displayed in Fig. 3(b). Inset of Fig. 3(b) is the electric field distribution of the two degenerate edge states. Figure 3(c) displays the topological corner state of the photonic crystal.

Figure 3(d) demonstrates the selective excitation of the topological edge states with opposite propagation directions. The excitation source for the right-going wave is made up of a point source of amplitude $1 + i$. The excitation source for the left-going wave is made up by shifting the right-going source of \mathcal{L} with the amplitude of $1 - i$. It is seen that in Fig. 3(d), by applying \mathcal{S} operation to the source, topological edge states with opposite propagation directions can be achieved. The excitation frequency is around 1.744 [GHz].

In summary, we propose a type of topological insulator imposed by spatial symmetry \mathcal{L} and time reversal symmetry K , which goes beyond the traditional band inversion scenario. As the nontrivial topology discussed is insensitive to hopping amplitudes and onsite energies, it opens a new venue for discovering materials hosting topological unidirectional edge modes and corners modes, which is essential for developing topological quantum computers.

ACKNOWLEDGMENTS

This work is supported by NSFC Grant No. 12074205 and NSFZP Grant No. LQ21A040004.

* ruserzzz@gmail.com

- [1] M. Z. Hasan and C. L. Kane, *Colloquium* : Topological insulators, *Rev. Mod. Phys.* **82**, 3045 (2010).
- [2] X.-L. Qi and S.-C. Zhang, Topological insulators and superconductors, *Rev. Mod. Phys.* **83**, 1057 (2011).
- [3] A. Bansil, H. Lin, and T. Das, *Colloquium* : Topological band theory, *Rev. Mod. Phys.* **88**, 021004 (2016).
- [4] Y. Hatsugai, Chern number and edge states in the integer quantum hall effect, *Phys. Rev. Lett.* **71**, 3697 (1993).
- [5] L. Fu and C. L. Kane, Time reversal polarization and a Z_2 adiabatic spin pump, *Phys. Rev. B* **74**, 195312 (2006).
- [6] Y. Hwang, J. Ahn, and B.-J. Yang, Fragile topology protected by inversion symmetry: Diagnosis, bulk-boundary correspondence, and Wilson loop, *Phys. Rev. B* **100**, 205126 (2019).
- [7] A. Bouhon, A. M. Black-Schaffer, and R.-J. Slager, Wilson loop approach to fragile topology of split elementary band representations and topological crystalline insulators with time-reversal symmetry, *Phys. Rev. B* **100**, 195135 (2019).
- [8] Z. Wang, L. Dong, C. Xiao, and Q. Niu, Berry curvature effects on quasiparticle dynamics in superconductors, *Phys. Rev. Lett.* **126**, 187001 (2021).
- [9] F. Liu and K. Wakabayashi, Novel topological phase with a zero berry curvature, *Phys. Rev. Lett.* **118**, 076803 (2017).
- [10] W. A. Benalcazar, B. A. Bernevig, and T. L. Hughes, Quantized electric multipole insulators, *Science* **357**, 61 (2017).
- [11] W. A. Benalcazar, B. A. Bernevig, and T. L. Hughes, Electric multipole moments, topological multipole moment pumping, and chiral hinge states in crystalline insulators, *Phys. Rev. B* **96**, 245115 (2017).
- [12] M. Ezawa, Higher-order topological insulators and semimetals on the breathing kagome and pyrochlore lattices, *Phys. Rev. Lett.* **120**, 026801 (2018).
- [13] F. Liu, H.-Y. Deng, and K. Wakabayashi, Helical topological edge states in a quadrupole phase, *Phys. Rev. Lett.* **122**, 086804 (2019).
- [14] B. A. Bernevig, T. L. Hughes, and S.-C. Zhang, Quantum spin hall effect and topological phase transition in HgTe quantum wells, *Science* **314**, 1757 (2006).
- [15] L. Michel and J. Zak, Connectivity of energy bands in crystals, *Phys. Rev. B* **59**, 5998 (1999).
- [16] B. Bradlyn, L. Elcoro, J. Cano, M. G. Vergniory, Z. Wang, C. Felser, M. I. Aroyo, and B. A. Bernevig, Topological quantum chemistry, *Nature* **547**, 298 (2017).
- [17] H. C. Po, H. Watanabe, and A. Vishwanath, Fragile topology and wannier obstructions, *Phys. Rev. Lett.* **121**, 126402 (2018).
- [18] S. Nie, Y. Qian, J. Gao, Z. Fang, H. Weng, and Z. Wang, Application of topological quantum chemistry in electrides, *Phys. Rev. B* **103**, 205133 (2021).
- [19] Y. Xu, L. Elcoro, Z.-D. Song, M. G. Vergniory, C. Felser, S. S. P. Parkin, N. Regnault, J. L. Mañes, and B. A. Bernevig, Filling-enforced obstructed atomic insulators, *Phys. Rev. B* **109**, 165139 (2024).
- [20] W. P. Su, J. R. Schrieffer, and A. J. Heeger, Solitons in polyacetylene, *Phys. Rev. Lett.* **42**, 1698 (1979).
- [21] F. Liu, Analytic solution of the n -dimensional Su-Schrieffer-Heeger model, *Phys. Rev. B* **108**, 245140 (2023).
- [22] F. D. M. Haldane, Model for a quantum hall effect without Landau levels: Condensed-matter realization of the "parity anomaly", *Phys. Rev. Lett.* **61**, 2015 (1988).
- [23] C. L. Kane and E. J. Mele, Quantum spin hall effect in graphene, *Phys. Rev. Lett.* **95**, 226801 (2005).
- [24] K. Shiozaki, M. Sato, and K. Gomi, Z_2 topology in nonsymmorphic crystalline insulators: Möbius twist in surface states, *Phys. Rev. B* **91**, 155120 (2015).
- [25] R. Xiao and Y. X. Zhao, Revealing the spatial nature of sublattice symmetry, *Nature Commun.* **15**, 3787 (2024).
- [26] W. A. Benalcazar, T. Li, and T. L. Hughes, Quantization of fractional corner charge in C_n -symmetric higher-order topological crystalline insulators, *Phys. Rev. B* **99**, 245151 (2019).